Published in final edited form as:

Acta Biomater. 2015 June ; 19: 1–9. doi:10.1016/j.actbio.2015.03.017.

Synthetic bone mimetic matrix-mediated in situ bone tissue formation through host cell recruitment

Yu-Ru Shih[a,1], **Ameya Phadke**[a,1], **Tomonori Yamaguchi**[b,c,1], **Heemin Kang**[a], **Nozomu Inoue**[c], **Koichi Masuda**[b,*], and **Shyni Varghese**[a,*]

[a]Department of Bioengineering, Jacobs School of Engineering, University of California, San Diego, La Jolla, CA 92093, USA

[b]Department of Orthopaedic Surgery, School of Medicine, University of California, San Diego, La Jolla, CA 92093, USA

[c]Department of Biomedical Engineering, Graduate School of Life and Medical Sciences, Doshisha University, Kyoto, Japan

Abstract

Advances in tissue engineering have offered new opportunities to restore anatomically and functionally compromised tissues. Although traditional tissue engineering approaches that utilize biomaterials and cells to create tissue constructs for implantation or biomaterials as a scaffold to deliver cells are promising, strategies that can activate endogenous cells to promote tissue repair are more clinically attractive. Here, we demonstrate that an engineered injectable matrix mimicking a calcium phosphate (CaP)-rich bone-specific microenvironment can recruit endogenous cells to form bone tissues *in vivo*. Comparison of matrix alone with that of bone marrow-soaked or bFGF-soaked matrix demonstrate similar extent of neo-bone formation and bridging of decorticated transverse processes in a posterolateral lumbar fusion rat model. Synthetic biomaterials that stimulate endogenous cells without the need for biologics to assist tissue repair could circumvent limitations associated with conventional tissue engineering approaches, including *ex vivo* cell processing and laborious efforts, thereby accelerating the translational aspects of regenerative medicine.

Graphical Abstract

*Corresponding author. Department of Bioengineering, University of California San Diego, 9500 Gilman Drive, MC 0412, La Jolla, CA 92093, United States. Phone: +1 858 822-7920, Fax: +1 858 534 5722, svarghese@ucsd.edu (S. Varghese)., Department of Orthopaedic Surgery, University of California San Diego, komasuda@ucsd.edu (K. Masuda).

[1]Y.R.S, A.P, and T.Y contributed equally to this work

Disclosures

Authors declare no conflict of interest.

Appendix A. Supplementary data

Supplementary Figure S1

Supplementary Movie S1–S3

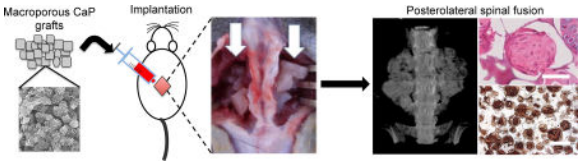

Keywords

Biomimetic materials; bone grafts; posterolateral fusion; spine; biomineralization; endogenous cell recruitment

1. Introduction

Bone grafting has become an increasingly prevalent procedure. Bone is the third most transplanted tissue after skin and blood with over 500,000 bone grafting procedures performed annually in the United States alone [1]. A variety of procedures necessitate the use of bone grafts: these include spinal fusion procedures and large bone defects arising from trauma or excision of large segments of bone due to infection or tumor invasion. Among these, spinal fusions are increasingly predominant and the frequency and healthcare costs associated with spinal fusion have increased at a higher rate than other common inpatient procedures [2]. Spinal fusion procedures are typically used to treat conditions arising from damage to the intervertebral disc, nerve compression, and spondylolistheses, among others.

Although autograft remains the gold standard, associated comorbidities and limited supply continue to motivate developments of alternative strategies for spinal fusion. Tissue engineering strategies involving biologics such as osteoprogenitors and recombinant proteins have been touted as powerful approaches to treat non-uniform defects. These approaches often utilize a cell-laden three-dimensional (3-D) scaffold, which provides structural support and instructive cues. One such strategy involves delivery of osteoinductive growth factors, such as recombinant bone morphogenetic proteins (BMPs), with recombinant human BMP-2 (rhBMP-2) and BMP-7 (rhBMP-7) currently approved for clinical use in various parts of the world [3, 4]. While BMPs are powerful inducers of bone tissue formation and delivery of BMPs leads to favorable clinical outcome through bone regeneration, the BMP-mediated bone tissue repair suffers from a number of shortcomings. These limitations include the high cost associated with the large dose of BMPs required as well as the accompanying side effects, such as respiratory effects, ectopic bone formation, local bone resorption at the implant site, and even an increase in the risk for cancer [5]. Other biologic additives such as exogenous cells [6], demineralized bone [7], bone marrow aspirate [8], platelet-rich plasma [9] or bFGF [10] have been used in combination with biomaterials or bone grafts to improve the therapeutic outcome in animal models. Recently, silicated calcium phosphates mixed with bone marrow aspirate have shown to promote posterolateral lumbar fusion in patients [11]. A report by Acharya *et al.* suggest that in the absence of biologic additives such as bone marrow, exogenous cells or demineralized bone matrix, synthetic calcium phosphates do not promote posterolateral fusion in patients [12]. Although such biomaterial-assisted inclusion of biologics to repair bone tissue is highly potent, new approaches that are cost-

effective and pose minimal side effects are warranted by developing biomaterials that can recruit endogenous cells and direct their differentiation into osteoblasts to form functional bone tissue.

We have recently shown that biomineralized matrices of poly(ethylene glycol) diacrylate-co-N-acryloyl 6-aminocaproic acid (PEGDA-co-A6ACA) promote osteogenic differentiation of human mesenchymal, embryonic stem cells, and induced pluripotent stem cells *in vitro* in growth medium devoid of any osteogenic-inducing factors [13–16]. We also showed that when subcutaneously implanted in rats, these materials contributed to ectopic bone formation by recruiting endogenous cells [17]. In this study, we examined the potential of these engineered matrices, emulating the calcium phosphate (CaP)-rich bone environment, (hereafter referred to as grafts) for their ability to induce bone formation and assist spinal fusion in rats. In addition to grafts alone, we also examined grafts supplemented with bone marrow flush or bFGF. Germane to our previous findings, the results described here show that the biomineralized material alone supported bone formation and assisted bridging of decorticated transverse process in a rodent.

2. Materials and Methods

2.1 Synthetic grafts

Formulation of the synthetic graft: Porous PEGDA-co-A6ACA hydrogels were prepared using a template-leaching method similar to that previously described [15, 16]. Briefly, 110 mg of polymethyl methacrylate (PMMA) microspheres (mean diameter: 165 μm) (Bangs Laboratories, MI) were poured into cylindrical polypropylene molds measuring 7 mm in diameter and tapped vigorously for 20–30 seconds to ensure optimal packing of microspheres. The microsphere-filled molds were sintered at 140°C for 26 hours and allowed to cool to room temperature for at least 4 hours. A precursor solution to create the polymer network was prepared by adding 20% poly(ethylene glycol)-diacrylate (PEGDA; M_n: 3.4 kDa; [w/v]) to a 0.5 M solution of N-acryloyl 6-aminocaproic acid (A6ACA) in 0.5 M NaOH and chilled on ice for 15 minutes. Polymerization was initiated by the addition of 0.5% ammonium persulfate and 0.07% N,N,N’N’-tetramethylethylenediamine. Approximately 0.110 ml of the precursor solution was poured into each PMMA mold and vacuum-infiltrated by cycling between ambient pressure and 28 in Hg vacuum every 5 minutes, with 3 cycles. The infiltrated samples were allowed to polymerize under humid conditions at 37°C for 2 hours. PMMA templates were removed by washing in acetone for 3 days (with two daily changes of solution), and subsequently immersing the hydrogels in decreasing concentrations of acetone in deionized (DI) water (90%, 70%, 30%, 0%) for 24, 12, 6 and 6 hours, respectively. The porous hydrogels were washed in deionized (DI) water for at least 3 days with three daily changes of water to remove traces of acetone, and then scraped to remove any thin non-porous layer at the surface and dried at 37°C for 24 hours.

The grafts were mineralized using a previously described procedure with some modifications [13, 17, 18]. Briefly, the macroporous hydrogels were re-swollen in simulated body fluid (m-SBF), prepared as detailed previously [19] for 12 hours, minced into pieces with a surgical scalpel, and then mineralized by immersion in 40 mM Ca^{2+}/24 mM PO_4^{3-} (pH = 5.2) under vacuum to ensure optimal infiltration of the solution into the scaffold

interior for 1 hour. Excess solution was removed from the graft pores by gently pressing on a paper towel, and the grafts were immersed in fresh m-SBF for an additional 48 hours. The mineralized grafts were washed briefly in sterile PBS for 6 hours to remove excess m-SBF from the pores, loaded into 1-ml syringes (Terumo Medical, Inc.) (0.3 ml/syringe), frozen at −80°C and lyophilized for 48 hours.

2.2 Scanning electron microscopy (SEM) and energy dispersive spectra (EDS)

Mineralized matrices were imaged with SEM to investigate the morphology of the mineralized matrices. Samples were rinsed in DI water for 5 minutes to remove unbound ions, cut into thin slices, flash-frozen, and lyophilized. Samples were coated with Iridium for 7 seconds in the sputter (Emitech, K575X) and imaged with SEM (Philips XL30 ESEM). EDS analysis was performed to determine the composition of the minerals using an integrated EDS system and ICA software to quantify Ca/P atomic ratio from elemental spectra.

2.3 Surgical procedure

Twenty-three male athymic rats (*rnu/rnu*, Harlan) weighing 250–300 g used for the study were in compliance with the NIH Guide for Care and Use of Laboratory Animals with the approval of the Institutional Animal Care and Use Committee at the University of California, San Diego. Two of the 23 rats were used as bone marrow donors. After sacrifice, the femurs of these two rats were removed and cleaned of soft tissue remnants. The ends of the femur were cut and flushed four times with DMEM (GIBCO) (4 ml/femur total). The concentration of viable mononucleated cells was determined to be 1.1×10^7 cells/ml. The remaining twenty-one rats were used for implantation. The rats were anesthetized with an intramuscular injection of approximately 0.45 ml of ketamine-xylazine. L4-L5 transverse processes were exposed through a dorsal midline skin incision and paravertebral muscle separation, stripped of periosteum by scraping, and decorticated with a burr until bleeding was observed from the transverse processes. 0.3 ml of the lyophilized synthetic graft was rehydrated for 1 minute in either physiological saline, bone marrow (BM) flush, or basic fibroblast growth factor (bFGF; 10 ng/ml) in saline and placed between the transverse processes in the fusion bed on each side of the spine. Seven rats received BM flush-soaked grafts, seven received bFGF-soaked grafts, while the remaining seven received grafts soaked in saline. The muscle pouch was closed with resorbable 4-0 Vicryl sutures and the skin was closed with staples. Buprenorphine (0.03 – 0.05 mg/kg) was administered for relieving postoperative pain and the animals were allowed access to food and water *ad libitum*. At 8 weeks, the rats were euthanized by CO_2 and cervical dislocation.

2.4 Measurement of bFGF retention on grafts

Lyophilized synthetic grafts (0.3 ml) were rehydrated for 1 minute in bFGF solution (500 μg/ml). The concentration of bFGF remaining in the unbound bFGF solution was measured with a UV-Vis Spectrophotometer (Nanodrop 2000, Thermo Scientific). The percentage of bound bFGF was calculated after subtraction of bound bFGF from the original bFGF solution.

2.5 Radiographic monitoring

Bone formation in the host was monitored as a function of time through live imaging. Anterior-posterior (AP) digital radiographs (NAOMI; 365 dpi; 71 μm pixel size; 50 kVp; 10 μAs) were acquired at 0, 2, 4, 6, and 8 weeks post-implantation. Post-sacrifice, animals were also imaged via high-resolution X-ray films using a tabletop Faxitron X-ray machine.

2.6 Micro-computed tomography

Animals were imaged via whole-body micro-computed tomography (μCT) (Skyscan1076, Skyscan, Belgium) in live animals at 8 weeks (pixel size: 36 μm; 100 kV; 1.0-mm Al filter) under anesthesia (2% isofluorane). Scans were reconstructed using NRecon software and analyzed via CTAn and DataViewer software (Skyscan). Bone (or hard tissue) volume percentage was calculated for each animal at 8 weeks from the reconstructed μCT scans using CTAn software. Bone morphometry was assessed as percentage of mineral volume compared to total graft volume (BV/TV) with CTAn software. Briefly, to selectively account for positive signals from minerals by eliminating background, a thresholding value was determined for native trabecular bone using the Otsu Threshold Method.

The fusion mass region on each side of the spine (left and right) was then isolated as a region of interest in each slice via visual inspection and the pre-determined threshold was applied. Bone density was quantified as percentage of volume occupied by bone (hard tissue with a pixel value exceeding the threshold) as compared to total tissue volume for each side. For each animal, bone volume percentage was expressed as the average of the bone volume percentage in the left and right side fusion mass, respectively.

2.7 Bone labeling with calcein fluorochrome

Calcein fluorochrome (Sigma Aldrich) labeling was used to identify newly calcified/forming bone tissues; freshly prepared calcein reagent was used for the injection. Briefly, calcein powder was dissolved in 2% $NaHCO_3$ (diluted in physiological saline) to make a 3 mg/ml stock solution and filter-sterilized using a 0.22-μm filter. The calcein solution was loaded into 3-ml syringes and injected into the athymic rats subcutaneously at 15 mg/kg body weight at week 6 (2 weeks before sacrifice at week 8).

2.8 Histology

Following sacrifice, the spines were excised from the animals along with surrounding soft tissue and fixed in 10% buffered formalin. Samples were decalcified for 1–2 weeks using Cal-EXII according to the manufacturer’s instructions. Decalcified samples were embedded in methyl methacrylate, sectioned, and stained using hematoxylin and eosin (H&E). For immunohistochemical (IHC) staining of osteocalcin, rehydrated paraffin-embedded sections were washed in PBS, blocked, and incubated overnight with primary antibodies against osteocalcin (1:100; mouse monoclonal; Abcam) at 4°C. Following thorough washes, sections were immersed in 3% hydrogen peroxide (Acros Organics) and washed in PBS containing 0.1% Tween 20 (v/v). Sections were exposed to horseradish peroxidase (HRP)-conjugated secondary antibodies (1:100; goat anti-mouse, Santa Cruz Biotechnology) at room temperature for 60 minutes. After several washes, sections were developed in 3-3’ diaminobenzidine (DAB) peroxidase substrate (Vector Laboratories) for 10 minutes.

Sections were imaged under a microscope in color mode under H-filter. Rat skin tissue was used as a negative control.

2.9 Manual Palpation

Following sacrifice, spines were extracted from animals and manually palpated to evaluate fusion. Movement of fused adjacent vertebra was compared to movement of unfused adjacent vertebra [20]. Spines were graded on a scale of 1–4, with 1 representing no fusion with substantial movement, 2 representing limited fusion with reduced movement, 3 representing substantial fusion with minimal movement, and 4 representing complete fusion with no detectable movement.

2.10 Lateral Bending

In addition to manual palpation and radiographic evaluation, fusion was evaluated using a custom-designed approach [21]. Briefly, explanted spines were placed in a custom-designed device capable of displacement-controlled lateral bending. Spines were anchored at the sacrum by three set screws and the L1 vertebral body was placed in the loading mechanism and allowed displacement of samples in the medial-lateral direction resulting in cantilever bending. Specifically, the L1 vertebral body was moved to three specific positions: bent left (−10 mm), neutral (0 mm), and bent right (+10 mm). Supplementary Figure S1 depicts right bending as an example. In each position, the spine was imaged using μCT (pixel size: 18 μm, 70 kV, 1.0-mm Al filter), and converted to 3-D models using Mimics software. Six degrees-of-freedom 3-D segmental movements (3 rotational and 3 translational) were analyzed via Volume-Merge method [22].

2.11 Statistical analysis

Statistical analyses were carried out using Graphpad Prism 5. One-way analysis of variance (ANOVA) with Tukey post-hoc test was used to compare multiple groups. In the figures, groups with statistical significance are represented using different letters, i.e. groups with “a” are statistically significant to those with “b”. The *p*-values were obtained from each test.

3. Results

3.1 Macroporous mineralized grafts

The development and detailed characterization of the biomineralized matrix has been published previously [14, 15, 17, 18]. SEM characterization confirmed that the grafts exhibited interconnected pore structure (Fig. 1A). The matrix bound minerals had a plate-like morphology (Fig. 1A, inset). The elemental dispersive spectra (EDS) analysis of the graft revealed the presence of CaP minerals with a Ca/P ratio of 1.44 in the mineralized macroporous hydrogels (Fig. 1B). XRD analyses of the mineralized matrices suggested presence of a mixture of crystalline and semicrystalline minerals [18]. The CaP minerals of the mineralized matrix undergo a dynamic dissolution-precipitation responding to the Ca^{2+} and PO_4^{3-} in the milieu [15].

The overall development of the grafts and their *in vivo* implantation is depicted in Figure 1C. Minced porous materials were mineralized, lyophilized in 1-ml syringes, and rehydrated

for 1 minute with either saline, basic fibroblast growth factor (bFGF) solution, or bone marrow (BM) flush before being injected into the surgically created fusion beds in rats. The growth factor bFGF was chosen because a number of studies have shown its role in promoting bone formation [23–25]; furthermore, silencing the *bFGF* gene results in decreased bone formation [26]. Although the exact amount of bFGF adsorbed onto the mineralized grafts is unknown, our measurements indicate more than 80% of bFGF can be adsorbed onto the mineralized grafts from the soaking solution. The porous graft materials were injected into the decorticated transverse processes in the fusion bed on each side of the spine (white arrow). The ability of the grafts to support bone formation and assist fusion of the transverse processes was determined as a function of post-implantation time.

3.2 Radiographic analysis of hard tissue formation and mineral density

The presence of hard tissue formation in saline-soaked, bFGF-soaked, and BM flush-soaked grafts were imaged by X-ray radiography (Fig. 2A). No adverse reaction to the grafts was observed in any of the animals throughout the study period. X-ray radiographic analysis of the animals immediately post-implantation revealed that the grafts were not visible in any of the animals (Fig. 2A; red asterisks). In contrast to the immediate post-implantation radiographs, fusion masses of newly formed hard tissues were visible in some of the animals as early as 2 weeks (4 animals out of 7 in each group). By 4 weeks, all animals showed clear evidence of hard tissue formation, with progressively increasing mineral density observed at 6 and 8 weeks, respectively. Remarkably, *de novo* hard tissue formation was observed irrespective of whether the implants were soaked in saline, bFGF, or BM flush (Fig. 2A). Also, no observable difference could be discerned between animals within the three groups.

Micro-computed tomography (μCT) analyses corroborated the radiographic findings. μCT analyses after 8 weeks of implantation revealed hard tissue formation in all animals treated with implants irrespective of whether they were infused with saline, bFGF, or BM. Visual inspection of μCT scans indicated that the formation of new bone was restricted to the grafts (Fig. 2B and Supplementary Movies S1–3). Additionally, examination of transaxial cross-sectional views of the reconstructed 3-D images revealed that the newly formed bone is bridged with the decorticated transverse processes (Fig. 2B). Bone morphometric analysis from μCT imaging at 8 weeks post-implantation revealed the percentage of mineralized hard tissue, relative to total graft volume, to be 51% for saline group, 59% for bFGF group, and 54% for BM group, with bFGF significantly higher than saline and BM groups (Fig. 2C). While the graft fragments showed excellent hard tissue formation, spaces between the fragments of the grafts showed more sparse bone formation and less calcification.

3.3 Histological analysis of bone formation

Calcein labeling for calcium incorporation into newly formed tissue at 8 weeks post-implantation revealed consistent calcification with positive calcein signals for saline, bFGF, and BM groups, respectively (Fig. 3A). H&E staining for the decalcified sections within the fusion masses at 8 weeks post-implantation revealed woven bone matrix with osteoblast-like lining cells in all experimental groups (Fig. 3B; blue arrows). The bone tissue formation was further confirmed by immunostaining for osteocalcin, a bone specific protein. Significant osteocalcin immunostaining was detected in all the three groups: saline-, bFGF- and BM-

soaked groups (Fig. 3C). Lacunae-like cartilage structures were apparent in saline and BM groups (Fig. 3B; yellow arrows). No such cartilage-like structure was observed in grafts enriched with bFGF at the same experimental time point(s).

3.4 Evaluation of fusion through manual palpation

Despite its subjectivity, manual palpation has been touted as a gold standard for evaluation of spinal fusion in human patients [20]. Manual palpation of animals treated with the grafts revealed an average score of 2.9 for the saline group, 3.0 for the BM group, and 2.7 for the bFGF group, thus providing evidence of fusion in all groups, with no significant differences in fusion indices (Fig. 4A). In comparison, sham group (decortication only) consistently scored approximately 1, supporting the radiographic observations of lack of fusion and bone formation in the absence of exogenous grafts [21].

3.5 Lateral bending analysis of 3-D segmental movements

While the aforementioned measurements showed the formation of neo-bone tissue, it is important to quantitate the bridging of the neo-bone with the host transverse processes. To assess the functional integration of the neo-tissue with the native bone, 3-D segmental movements during lateral bending motions were determined. We quantified the 3-D segmental movements of the animals treated with implants after 8 weeks of implantation by using a technique developed by our group that involves lateral bending of the fused spines under controlled displacement along with a μCT-based 3-D kinematic analysis [21]. The total absolute value of rotation about the *x*-axis in lateral bending is defined as the 3-D lateral bending angular range of motion (ROM). A low ROM indicates bridging of the neo-bone tissue with the host transverse processes, thereby spinal fusion. In this study, spines treated with the synthetic grafts soaked with saline and BM showed a statistically significant reduction in lateral bending angular ROM compared to the sham surgery group ($p<0.05$), with lateral bending angular ROMs of approximately 7.54±2.63° and 8.16±2.50° for the saline and BM groups, respectively, compared to 12.44±2.10° observed for the sham surgery group (Fig. 4, B and C). The significant reduction in mobility for the saline and BM groups compared to sham suggests that the grafts were fused with the transverse processes through the bridging of newly formed bone. On the other hand, the bFGF group did not significantly reduce mobility compared to sham. Additionally, no significant differences were observed between the saline and BM groups, further supporting the results from the μCT and histological analyses that the saline-soaked grafts were able to promote bone tissue formation and fusion to a similar extent as the BM flush-soaked grafts.

4. Discussion

In this study, we examined the ability of synthetic biomineralized matrices to support *in vivo* bone formation and bridging of decorticated transverse process in a rodent model with the addition of BM flush or bFGF. Live radiographic imaging was used to monitor hard tissue formation for up to 8 weeks. X-ray images and μCT analyses of the grafts immediately following implantation showed the grafts themselves were not visible suggesting that the biomineralized matrices contained only small amounts of minerals. The subsequent fusion masses of hard tissue observed at the implantation site starting 2 weeks post-implantation

can thus be solely attributed to the formation of new hard tissue and not an artifact due to visualization of the mineralized grafts themselves.

H&E staining and calcein labeling, together with the immunostaining for osteocalcin, further confirm hard neo-bone tissue, which was restricted to the graft. It is important to note that several of the large graft fragments in the μCT images showed relatively higher calcification at the periphery compared to the center of the fragment, while smaller fragments showed similar levels of calcification throughout the entire fragment. The formation of an exterior shell has often been reported during bone induction in soft tissues, particularly when calcium phosphate matrices are used either in isolation or as carriers for osteoinductive growth factors [27, 28]. The histological analyses showed extensive tissue formation throughout the graft irrespective of the size of the fragments. Furthermore, the histological analyses showed bone formation even in graft fragments located in the center of the fusion mass, away from the transverse processes. The majority of bone tissue appeared to resemble woven bone. The presence of cartilaginous matrix in grafts infused with saline and bone marrow groups suggests that the bone tissue formation, as evident by bone matrix and immunostaining for osteocalcin, followed endochondral ossification for these groups.

While manual palpation may seem fairly subjective and susceptible to inter-observer and intra-observer variability, studies using manual palpation to assess posterolateral intertransverse process spinal fusion indeed show correlation with other methods, such as fine detail radiography and μCT for evaluation of fusion [29]. The results of manual palpation in this study indicate that all grafts irrespective of the biological additives were able to promote bridging of the graft assisted neo-bone tissue with the native transverse process). Results from the lateral bending quantitative analyses corroborated findings from the manual palpation. As evident from the 3-D lateral bending analyses, the saline-, and BM flush-infused grafts not only promoted neo-bone tissue formation, but also led to a 40% reduction in angular range of motion when compared to the corresponding sham surgery. Mechanical characterization thus corroborated the μCT and histological findings that the synthetic grafts assisted the bridging of the transverse process.

The contribution of BM-infused and bFGF-infused grafts towards the neo-bone tissue formation is dependent upon the extent of adsorbed/bound biological materials. Bone marrow flush is comprised of a large number of cytokines, growth factors, and cells, including MSCs. Determining the composition and concentration of the biological components within the BM flush-infused grafts is a challenge. Previously, we have shown that incorporation of 6-aminocaproic acid (6ACA) moieties improves the protein and growth factor-binding ability of various materials, including the antifouling materials [30]. Synthetic matrices containing 6ACA moieties have also been shown to promote adhesion and growth of human mesenchymal stem cells [31]. Biomineralization should not have any negative effect on the ability of these materials to adsorb proteins and growth factors as a number of studies have shown that mineralization promotes adsorption of proteins and growth factors [32–34]. Measurements of bFGF adsorption onto the mineralized materials suggest that a majority of bFGF was adsorbed by the graft (>80%). This is consistent with other studies that showed high levels of bFGF adsorption by the CaP-based materials [35, 36].

It is particularly intriguing that the saline-soaked grafts lacking any biological additives promoted bone tissue formation similar to the grafts soaked with BM flush or bFGF, and that the material alone is osteoconductive. Osteoconduction may depend on the action of differentiated skeletal cells that may originate either in pre-existing osteoblasts or in cells recruited from precursor mesenchymal cells by osteoinduction [37]. Since we did not identify the cells that contributed to then neo-bone, the mineralized scaffolds either stimulated differentiation of recruited progenitor cells into osteoblasts or recruited endogenous osteoblasts *per se*, leading to the deposition of bone matrix and bone formation. The presence of host cells in the grafts is likely facilitated by bleeding of the transverse processes during surgical implantation of grafts. This suggests that the biomineralized matrices used in this study are osteoinductive and the material can convert osteoprogenitors into osteoblasts through endochondral ossification. Synthetic calcium-phosphate materials that facilitate ectopic bone formation in the absence of biologics or exogenous cells as demonstrated in our study have been observed by others [38–43]. The ability of biomineralized matrices to promote ectopic bone tissue formation could be attributed to physicochemical cues arising from the mineralized matrix. The biomineralized matrices used in this study contained apatite-like CaP minerals that can be easily dissociated into Ca^{2+} and PO_4^{3-} ions [44]. We and others have demonstrated the dissolution-precipitation of mineralized materials that leads to increased local Ca^{2+} and PO_4^{3-} concentrations within the immediate microenvironment of matrices promote osteogenic differentiation of osteoprogenitor cells *in vitro*, [13, 14, 45–47] and could play a role in osteoinduction by mineralized materials *in vivo* [13, 45, 48, 49]. Crystalline CaP minerals have demonstrated increasing dissolution rates in the order of hydroxyapatite (HA), biphasic calcium phosphate (BCP), and tricalcium phosphate (TCP) [47, 50] which proportionally promoted osteogenic differentiation of MSCs [51]. A direct comparison between HA, BCP, and TCP showed enhanced bone regeneration by TCP compared with BCP in the skeletal sites and no bone formation with HA [47]. In addition, the mineralized phase could also promote the selective adsorption and subsequent release of pro-angiogenic and pro-osteogenic growth factors from the surrounding physiological environment, such as vascular endothelial growth factors (VEGFs) and bone morphogenetic proteins (BMPs) [52–54], leading to their accumulation within the implant and fusion bed for osteoinduction.

Given the relative scarcity of biologic-independent synthetic matrices for bone induction, the consistent osteoinductivity displayed by the mineralized PEGDA-co-A6ACA grafts is highly encouraging and could potentially allow for their use in spinal fusion procedures without the need for any biologic additives, such as bone marrow aspirate, platelet-rich plasma, growth factors, and others. Synthetic materials that could promote bone tissue formation and fusion between native and neo-bone without the addition of biologics and exogenous cells are highly desirable and could be an alternative to current grafting strategies.

5. Conclusion

This work demonstrates the utility of novel synthetic bone grafts based on biomineralized porous matrices in an athymic rat posterolateral fusion model. Results from our study show that the biomineralized synthetic matrices were able to assist neo-bone tissue formation and promote posterolateral fusion as evidenced by radiographic, histological and lateral bending

analyses. These grafts were found to promote bone tissue formation and fusion irrespective of the presence of bone marrow flush or bFGF, as saline-soaked grafts *per se* were able to produce highly similar, statistically significant improvements when compared to sham surgery.

Supplementary Material

Refer to Web version on PubMed Central for supplementary material.

Acknowledgments

The authors gratefully acknowledge the financial support from National Institutes of Health (NIH, Grant 1 R01 AR063184-01A1).

References

1. Faour O, Dimitriou R, Cousins CA, Giannoudis PV. The use of bone graft substitutes in large cancellous voids: any specific needs? Injury. 2011; 42(Suppl 2):S87–90. [PubMed: 21723553]
2. Rajaee SS, Bae HW, Kanim LE, Delamarter RB. Spinal fusion in the United States: analysis of trends from 1998 to 2008. Spine. 2012; 37:67–76. [PubMed: 21311399]
3. Glassman SD, Howard J, Dimar J, Sweet A, Wilson G, Carreon L. Complications with recombinant human bone morphogenic protein-2 in posterolateral spine fusion: a consecutive series of 1037 cases. Spine. 2011; 36:1849–54. [PubMed: 20838369]
4. Bhatia, SK., Bhatia, SR. Bioactive Devices. In: Lee, S., Henthorn, D., editors. Materials in Biology and Medicine. Boca Raton, FL: CRC Press; 2012. p. 149-60.
5. Carragee EJ, Hurwitz EL, Weiner BK. A critical review of recombinant human bone morphogenetic protein-2 trials in spinal surgery: emerging safety concerns and lessons learned. The spine journal : official journal of the North American Spine Society. 2011; 11:471–91. [PubMed: 21729796]
6. Kai T, Shao-qing G, Geng-ting D. In vivo evaluation of bone marrow stromal-derived osteoblasts-porous calcium phosphate ceramic composites as bone graft substitute for lumbar intervertebral spinal fusion. Spine. 2003; 28:1653–8. [PubMed: 12897487]
7. Lee YP, Jo M, Luna M, Chien B, Lieberman JR, Wang JC. The efficacy of different commercially available demineralized bone matrix substances in an athymic rat model. Journal of spinal disorders & techniques. 2005; 18:439–44. [PubMed: 16189457]
8. Tay BK, Le AX, Heilman M, Lotz J, Bradford DS. Use of a collagen-hydroxyapatite matrix in spinal fusion. A rabbit model. Spine. 1998; 23:2276–81. [PubMed: 9820906]
9. Okamoto S, Ikeda T, Sawamura K, Nagae M, Hase H, Mikami Y, et al. Positive effect on bone fusion by the combination of platelet-rich plasma and a gelatin beta-tricalcium phosphate sponge: a study using a posterolateral fusion model of lumbar vertebrae in rats. Tissue engineering Part A. 2012; 18:157–66. [PubMed: 21819268]
10. Yoshida T, Sakamoto A, Tsukamoto N, Nakayama K, Iwamoto Y. Establishment of an animal model of a pasteurized bone graft, with a preliminary analysis of muscle coverage or FGF-2 administration to the graft. Journal of orthopaedic surgery and research. 2009; 4:31. [PubMed: 19650934]
11. Jenis LG, Banco RJ. Efficacy of silicate-substituted calcium phosphate ceramic in posterolateral instrumented lumbar fusion. Spine. 2010; 35:E1058–63. [PubMed: 20479699]
12. Acharya NK, Kumar RJ, Varma HK, Menon VK. Hydroxyapatite-bioactive glass ceramic composite as stand-alone graft substitute for posterolateral fusion of lumbar spine: a prospective, matched, and controlled study. Journal of spinal disorders & techniques. 2008; 21:106–11. [PubMed: 18391714]
13. Phadke A, Shih YR, Varghese S. Mineralized synthetic matrices as an instructive microenvironment for osteogenic differentiation of human mesenchymal stem cells. Macromolecular bioscience. 2012; 12:1022–32. [PubMed: 22760917]

14. Shih YR, Hwang YS, Phadke A, Kang H, Hwang NS, Caro EJ, et al. Calcium phosphate-bearing matrices induce osteogenic differentiation of stem cells through adenosine signaling. Proceedings of the National Academy of Sciences. 2014; 111:990–5.
15. Kang H, Wen C, Hwang Y, Shih YR, Kar M, Seo SW, et al. Biomineralized matrix-asssisted osteogenic differentiation of human embryonic stem cells. Journal of Materials Chemistry B. 2014; 2:5676–88.
16. Kang H, Shih YR, Hwang Y, Wen C, Rao V, Seo T, et al. Mineralized gelatin methacrylate-based matrices induce osteogenic differentiation of human induced pluripotent stem cells. Acta Biomaterialia. 2014
17. Phadke A, Hwang Y, Kim SH, Kim SH, Yamaguchi T, Masuda K, et al. Effect of scaffold microarchitecture on osteogenic differentiation of human mesenchymal stem cells. European Cells and Materials. 2013; 25:114–29. [PubMed: 23329467]
18. Phadke A, Zhang C, Hwang Y, Vecchio K, Varghese S. Templated mineralization of synthetic hydrogels for bone-like composite materials: Role of matrix hydrophobicity. Biomacromolecules. 2010; 11:2060–8. [PubMed: 20690714]
19. Oyane A, Kim HM, Furuya T, Kokubo T, Miyazaki T, Nakamura T. Preparation and assessment of revised simulated body fluids. Journal of biomedical materials research Part A. 2003; 65:188–95. [PubMed: 12734811]
20. Boden SD, Schimandle JH, Hutton WC. An experimental lumbar intertransverse process spinal fusion model. Radiographic, histologic, and biomechanical healing characteristics. Spine. 1995; 20:412–20. [PubMed: 7747224]
21. Yamaguchi T, Inoue N, Sah RL, Lee Y-P, Taborek AP, Williams GM, et al. Micro-computed tomography-based three-dimensional kinematic analysis during lateral bending for spinal fusion assessment in a rat posterolateral lumbar fusion model. Tissue Engineering Part C: Methods. 2014
22. Ochia RS, Inoue N, Renner SM, Lorenz EP, Lim TH, Andersson GB, et al. Three-dimensional in vivo measurement of lumbar spine segmental motion. Spine. 2006; 31:2073–8. [PubMed: 16915091]
23. Nagai H, Tsukuda R, Yamasaki H, Mayahara H. Systemic injection of FGF-2 stimulates endocortical bone modelling in SAMP6, a murine model of low turnover osteopenia. The Journal of veterinary medical science / the Japanese Society of Veterinary Science. 1999; 61:869–75.
24. Nakamura Y, Tensho K, Nakaya H, Nawata M, Okabe T, Wakitani S. Low dose fibroblast growth factor-2 (FGF-2) enhances bone morphogenetic protein-2 (BMP-2)-induced ectopic bone formation in mice. Bone. 2005; 36:399–407. [PubMed: 15777655]
25. Kimoto T, Hosokawa R, Kubo T, Maeda M, Sano A, Akagawa Y. Continuous administration of basic fibroblast growth factor (FGF-2) accelerates bone induction on rat calvaria--an application of a new drug delivery system. Journal of dental research. 1998; 77:1965–9. [PubMed: 9839783]
26. Montero A, Okada Y, Tomita M, Ito M, Tsurukami H, Nakamura T, et al. Disruption of the fibroblast growth factor-2 gene results in decreased bone mass and bone formation. The Journal of clinical investigation. 2000; 105:1085–93. [PubMed: 10772653]
27. Hartman EH, Vehof JW, Spauwen PH, Jansen JA. Ectopic bone formation in rats: the importance of the carrier. Biomaterials. 2005; 26:1829–35. [PubMed: 15576157]
28. Matsushita N, Terai H, Okada T, Nozaki K, Inoue H, Miyamoto S, et al. A new bone-inducing biodegradable porous beta-tricalcium phosphate. Journal of biomedical materials research Part A. 2004; 70:450–8. [PubMed: 15293319]
29. Yee AJ, Bae HW, Friess D, Robbin M, Johnstone B, Yoo JU. Accuracy and interobserver agreement for determinations of rabbit posterolateral spinal fusion. Spine. 2004; 29:1308–13. [PubMed: 15187630]
30. Kabra H, Hwang Y, Lim HL, Kar M, Arya G, Varghese S. Biomimetic Material-Assisted Delivery of Human Embryonic Stem Cell Derivatives for Enhanced In Vivo Survival and Engraftment. ACS Biomater Sci Eng. 2015; 1:7–12. [PubMed: 26280019]
31. Ayala R, Zhang C, Yang D, Hwang Y, Aung A, Shroff SS, et al. Engineering the cell-material interface for controlling stem cell adhesion, migration, and differentiation. Biomaterials. 2011; 32:3700–11. [PubMed: 21396708]

32. LeGeros RZ. Calcium phosphate-based osteoinductive materials. Chemical reviews. 2008; 108:4742–53. [PubMed: 19006399]
33. Alam MI, Asahina I, Ohmamiuda K, Takahashi K, Yokota S, Enomoto S. Evaluation of ceramics composed of different hydroxyapatite to tricalcium phosphate ratios as carriers for rhBMP-2. Biomaterials. 2001; 22:1643–51. [PubMed: 11374466]
34. Liu Y, Hunziker EB, Layrolle P, De Bruijn JD, De Groot K. Bone morphogenetic protein 2 incorporated into biomimetic coatings retains its biological activity. Tissue engineering. 2004; 10:101–8. [PubMed: 15009935]
35. Perez RA, Kim TH, Kim M, Jang JH, Ginebra MP, Kim HW. Calcium phosphate cements loaded with basic fibroblast growth factor: delivery and in vitro cell response. Journal of biomedical materials research Part A. 2013; 101:923–31. [PubMed: 22962037]
36. Midy V, Rey C, Bres E, Dard M. Basic fibroblast growth factor adsorption and release properties of calcium phosphate. Journal of biomedical materials research. 1998; 41:405–11. [PubMed: 9659610]
37. Albrektsson T, Johansson C. Osteoinduction, osteoconduction and osseointegration. European spine journal : official publication of the European Spine Society, the European Spinal Deformity Society, and the European Section of the Cervical Spine Research Society. 2001; 10(Suppl 2):S96–101.
38. Selye H, Lemire Y, Bajusz E. Induction of bone, cartilage and hemopoietic tissue by subcutaneously implanted tissue diaphragms. Dev Genes Evol. 1960; 151:572–85.
39. Pek YS, Gao S, Arshad MS, Leck KJ, Ying JY. Porous collagen-apatite nanocomposite foams as bone regeneration scaffolds. Biomaterials. 2008; 29:4300–5. [PubMed: 18706690]
40. Seyedjafari E, Soleimani M, Ghaemi N, Shabani I. Nanohydroxyapatite-coated electrospin poly(L-lactide) nanofibers enhance osteogenic differneitation of stem cells and induce ectopic bone formation. Biomacromolecules. 2010; 11:3118–25. [PubMed: 20925348]
41. Barradas AM, Yuan H, van der Stok J, Le Quang B, Fernandes H, Chaterjea A, et al. The influence of genetic factors on the osteoinductive potential of calcium phosphate ceramics in mice. Biomaterials. 2012; 33:5696–705. [PubMed: 22594974]
42. Cheng L, Duan X, Xiang Z, Shi Y, Lu X, Ye F, et al. Ectopic bone formation cannot occur by hydroxyapatite/β-tricalcium phosphate bioceramics in green fluorescent protein chimeric mice. Appl Surf Sci. 2012:262.
43. Kawai T, Anada T, Honda Y, Kamakura S, Matsui K, Matsui A, et al. Synthetic octacalcium phosphate augments bone regeneration correlated with its content in collagen scaffold. Tissue engineering Part A. 2009; 15:23–32. [PubMed: 18637727]
44. Phadke A, Zhang C, Hwang Y, Vecchio K, Varghese S. Templated mineralization of synthetic hydrogels for bone-like composite materials: role of matrix hydrophobicity. Biomacromolecules. 2010; 11:2060–8. [PubMed: 20690714]
45. Chai YC, Roberts SJ, Schrooten J, Luyten FP. Probing the osteoinductive effect of calcium phosphate by using an in vitro biomimetic model. Tissue engineering Part A. 2011; 17:1083–97. [PubMed: 21091326]
46. Chai YC, Roberts SJ, Van Bael S, Chen Y, Luyten FP, Schrooten J. Multi-level factorial analysis of Ca2+/Pi supplementation as bio-instructive media for in vitro biomimetic engineering of three-dimensional osteogenic hybrids. Tissue engineering Part C, Methods. 2012; 18:90–103. [PubMed: 21933019]
47. Yuan H, Fernandes H, Habibovic P, de Boer J, Barradas AM, de Ruiter A, et al. Osteoinductive ceramics as a synthetic alternative to autologous bone grafting. Proceedings of the National Academy of Sciences of the United States of America. 2010; 107:13614–9. [PubMed: 20643969]
48. Le Nihouannen D, Daculsi G, Saffarzadeh A, Gauthier O, Delplace S, Pilet P, et al. Ectopic bone formation by microporous calcium phosphate ceramic particles in sheep muscles. Bone. 2005; 36:1086–93. [PubMed: 15869915]
49. Muller P, Bulnheim U, Diener A, Luthen F, Teller M, Klinkenberg ED, et al. Calcium phosphate surfaces promote osteogenic differentiation of mesenchymal stem cells. Journal of cellular and molecular medicine. 2008; 12:281–91. [PubMed: 18366455]

50. Ducheyne P, Radin S, King L. The effect of calcium phosphate ceramic composition and, structure on in vitro behavior. I. Dissolution. Journal of biomedical materials research. 1993; 27:25–34. [PubMed: 8380596]

51. Barradas AM, Monticone V, Hulsman M, Danoux C, Fernandes H, Tahmasebi Birgani Z, et al. Molecular mechanisms of biomaterial-driven osteogenic differentiation in human mesenchymal stromal cells. Integrative biology : quantitative biosciences from nano to macro. 2013; 5:920–31. [PubMed: 23752904]

52. Lee JS, Suarez-Gonzalez D, Murphy WL. Mineral coatings for temporally controlled delivery of multiple proteins. Advanced materials. 2011; 23:4279–84. [PubMed: 22039597]

53. Yuan H, Zou P, Yang Z, Zhang X, De Bruijn JD, De Groot K. Bone morphogenetic protein and ceramic-induced osteogenesis. Journal of materials science Materials in medicine. 1998; 9:717–21. [PubMed: 15348928]

54. Suarez-Gonzalez D, Lee JS, Lan Levengood SK, Vanderby R Jr, Murphy WL. Mineral coatings modulate beta-TCP stability and enable growth factor binding and release. Acta Biomater. 2012; 8:1117–24. [PubMed: 22154864]

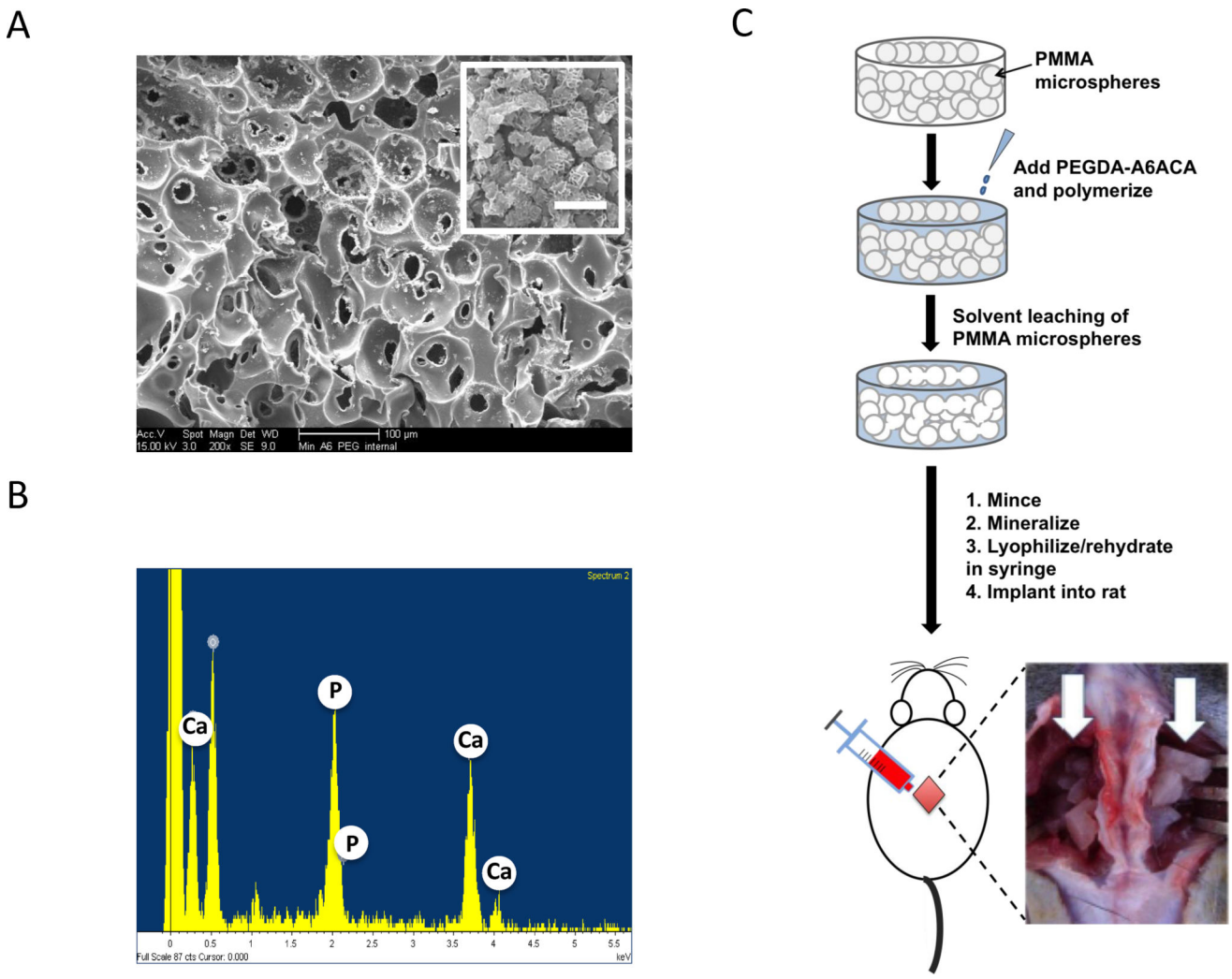

Figure 1.

Experimental procedure and characterization of mineralized macroporous matrices. (A) SEM images (inset shows high magnification image; Scale bar: 2 μm). (B) EDS analysis for calcium and phosphate ions of mineralized PEGDA-A6ACA hydrogels. (C) Schematic representation of the experimental procedure. Preparation of sintered template of PMMA microspheres (PMMA microspheres: grey spheres), polymerization of PEGDA-A6ACA hydrogel matrix (PEGDA-A6ACA: light blue mass) around the PMMA template, and the leaching of PMMA template to obtain porous hydrogel matrices (white). The porous hydrogels were minced and mineralized to obtain biomineralized grafts. The grafts were loaded into the syringe, lyophilized and rehydrated in saline, basic fibroblast growth factor (bFGF), or bone marrow (BM) flush prior to implantation. Implantation of grafts in nude rats for posterolateral fusion with white arrows pointing to grafts placed on either side of the spine at L4-L5 following decortication of transverse processes.

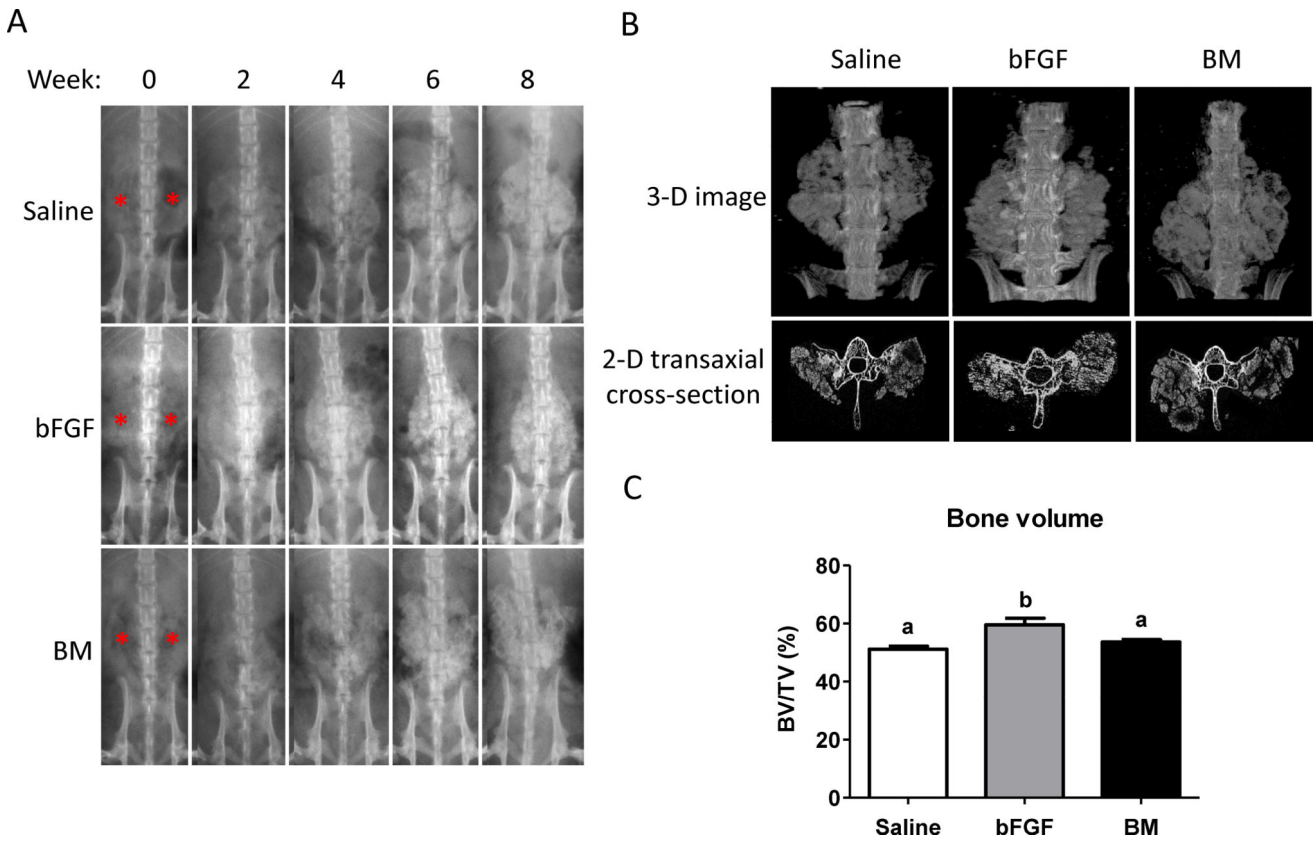

Figure 2.

X-ray and micro-computerized tomography (μCT) analysis. (A) Representative images from X-ray radiography of live animals receiving grafts infused with saline, basic fibroblast growth factor (bFGF), or bone marrow (BM) flush indicate hard tissue formation as a function of post-implantation time for up to 8 weeks. Red asterisks indicate the locations of implanted grafts at week 0. (B) Three-dimensional (3-D) micro-computerized tomography (μCT) and transaxial cross-sectional images at 8 weeks after graft implantation. (C) Bone density in fusion mass for saline-, bFGF-, and BM-soaked groups quantified from μCT images. Different letters represent statistical significances, where "*a*" is statistically significant compared to "*b*". Error bars represent standard error of the mean (n=7, $p<0.05$).

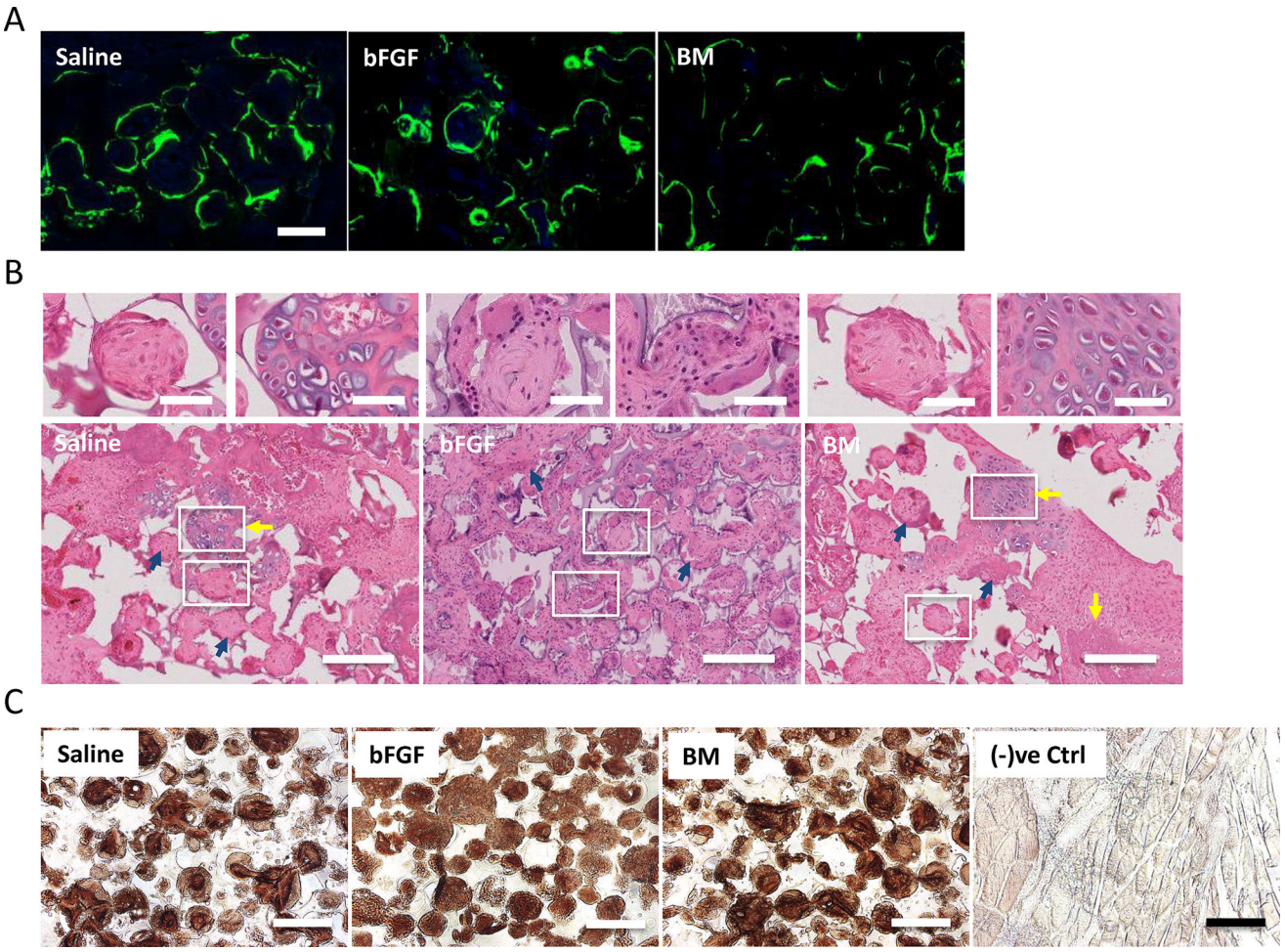

Figure 3.

Calcium deposition and histological staining for bone formation. (A) Calcein labeling suggests neo-calcium deposition in saline-, basic fibroblast growth factor (bFGF)-, and bone marrow (BM)-soaked grafts after 2 weeks of calcein uptake. Scale bar: 100 μm. (B) Hematoxylin-eosin (H&E) staining of grafts infused with saline, bFGF, and BM after 8 weeks of implantation for neo-bone tissue formation. Evidence of bone formation through endochondral ossification is evident in saline and BM groups (yellow arrows). Woven bone matrices with osteoblastic cells (blue arrows) were found in all groups. Scale bar: 200 μm. Magnified images on top are regions undergoing endochondral ossification or woven bone from regions highlighted by white borders. Scale bar: 50 μm. (C) Immunohistochemical staining for osteocalcin in saline-, bFGF-, and BM-soaked grafts after 8 weeks of implantation. Rat skin tissues were used as negative control [(−)ve Ctrl]. Scale bar: 200 μm.

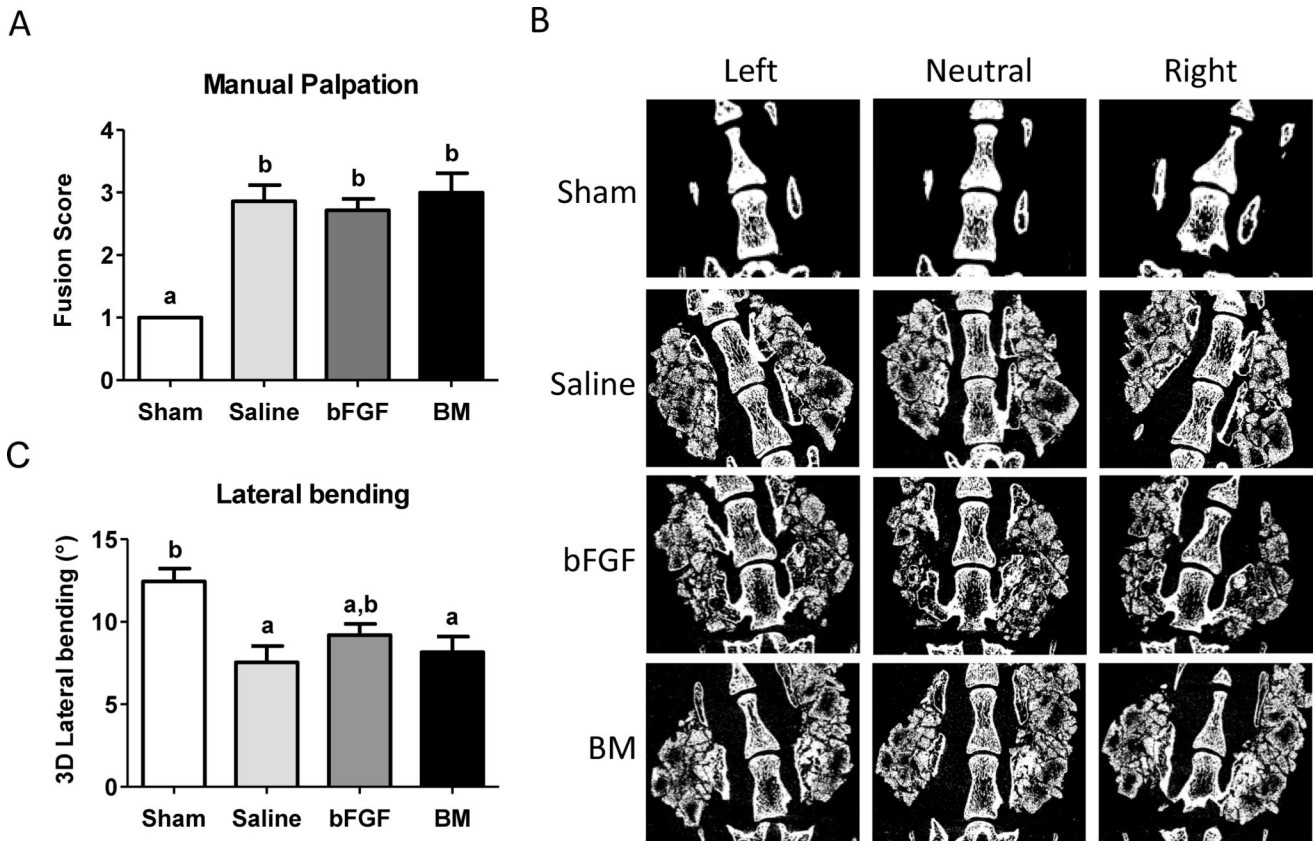

Figure 4.

Analysis for spinal fusion. (A) Fusion score generated from manual palpation for each group; saline-, basic fibroblast growth factor (bFGF)-, and bone marrow (BM)-soaked grafts, after 8 weeks of implantation. Different letters represent statistical significance. Error bars represent standard error of the mean (n=7, $p<0.05$). (B) Micro-computed tomography (μCT) of sham, saline-soaked, bFGF-soaked and BM-soaked biomineralized grafts undergoing lateral bending measurements. Representative images at different positions during measurements for various groups after 8 weeks post-implantation. (C) Three-dimensional (3-D) lateral bending angles of spine with saline-, bFGF-, and BM-soaked grafts compared to sham surgery. Different letters represent statistical significances with "*a*" statistically significant to "*b*". Error bars indicate standard error of the mean (n=7, $p<0.01$).